J. Fluid Mech. (2008), *vol.* 597, *pp.* 371–394.
doi:10.1017/S0022112007009822 Printed in the United Kingdom

The effect of gravity and cavitation on a hydrofoil near the free surface

ODD M. FALTINSEN AND YURIY A. SEMENOV

Centre for Ship and Ocean Structures, NTNU, N-7491 Trondheim, Norway

(Received 24 February 2007 and in revised form 24 October 2007)

A nonlinear analysis has been made to determine the effects of the free surface and transverse gravity field on the steady cavity flow past a shaped hydrofoil beneath the free surface. A closed cavity wake model has been proposed, and a method for the determination of an analytical function from its modulus and argument on the region boundary has been employed to derive the complex flow potential in a parameter plane. The boundary-value problem is reduced to a system of integral and integro-differential equations in the velocity modulus along the free boundaries and the velocity angle along the hydrofoil surface, both written as a function of parametric variables. The system of equations is solved through a numerical procedure, which is validated in the cases of a cavitating flat plate and non-cavitating shaped hydrofoils by comparison with data available in the literature. The results are presented in a wide range of Froude numbers and depths of submergence in terms of the cavity and free-surface shapes and force coefficients. The influences of the free surface and gravity on the aforementioned quantities are discussed. The limiting cavity size corresponding to zero cavitation number in the presence of gravity is found for various initial flow parameters.

1. Introduction

The study of flows past hydrofoils moving beneath the free surface started to receive much attention in the late 1950s owing to the development of high-speed hydrofoil craft, whose foilborne speed can be about twice as high as their hullborne speed (Acosta 1973). At present, the flow characteristics and motion stability are understood adequately for a subcavitating foil system. For a higher speed, an understanding of the interactions between the cavitation region and the free surface as well as motion stability is still inadequate (Faltinsen 2005). An extremely complicated question is ventilated cavitation, which may occur if the free surface comes close to the hydrofoil or the cavity boundary due to a wave disturbance of the free surface.

The problem of the cavity flow of a fluid with gravity past a submerged body involves two kinds of problem, which are presented in the literature separately. The first kind deals with the gravity flow of a fluid past submerged bodies, and the second kind deals with the cavity flow past hydrofoils beneath the free surface without gravity effects. The first kind is naturally connected with the theory of progressive gravity waves on the free surface generated downstream of a submerged body. Although theoretical methods for solving both kinds of problem are the same, the consideration of all of these features within the framework of a single problem is lacking in the literature.

Most of the theoretical studies for two-dimensional free-boundary flows are based on the complex-variable function theory. Since any analytical function satisfies the requirements of fluid incompressibility and zero vorticity, the problem is to find an analytical function which satisfies the given boundary conditions.

Early studies of the flow past a submerged body were based on the representation of the body as a dipole, vortex or source and the application of a linearized free-surface boundary condition (Havelock 1926; Kochin 1937). Keldysh & Lavrentiev (1935) considered the problem for thin fully wetted foils. Using linearized boundary conditions, they formulated a mixed boundary-value problem in the upper half-plane, whose solution is found using the Sokhotsky–Plemel formula. They obtained an elegant formula $C_D/C_L^2 = 0.5/Fn \exp[-2/Fn_h]$, where C_D and C_L are the drag and lift coefficients of the foil; Fn and Fn_h are the Froude numbers for the chord length of the foil and the depth of submergence h, respectively. The analysis of the total drag force of a hydrofoil (Faltinsen 2005) showed that the wave contribution to the drag–lift ratio is quite small at typical Froude numbers.

A linear theory of the flow past a submerged thin foil was developed by Hough & Moran (1969). They predicted a reduction in the lift force owing to gravity effects and showed that for $Fn \approx 10$ the gravity effects become negligible.

Nonlinear effects in the flow past a submerged body due to the body thickness and finite amplitude of free-surface waves were studied using the mathematical apparatus of matched asymptotic expansions. Tuck (1965) showed that nonlinear second-order effects become important if the cylinder is close to the free surface, the second-order effects caused by the nonlinearity of the free-surface condition being more important than the second-order effects related to the body boundary conditions. Giesing & Smith (1967) presented a method based on an integral representation of the flow potential generated by sources and vortices distributed along the hydrofoil surface. Each elementary singularity satisfies the exact boundary condition on the wetted body and the linearized boundary condition on the free surface. Since the problem is formulated in the physical plane, the method is applicable to determining the flow potential about one or more arbitrarily shaped bodies. Salvesen (1969) considered second-order effects in the free surface boundary condition for the flow about a submerged hydrofoil. He presented experimental data and confirmed Tuck's conclusion obtained for a cylinder that second-order effects in a free-surface boundary condition are important at relatively small submergences. Various theoretical formulations of the problem based on the method of matched asymptotic expansions were also presented by Dagan (1971) and Wilmot (1987). King & Bloor (1989) obtained an exact nonlinear solution for the flow around a Rankine-type submerged body formed by a source and sink. They used a conformal mapping transformation technique and derived, in particular, a nonlinear integro-differential equation in the velocity angle on the free surface. However, a complete nonlinear solution for an arbitrarily shaped hydrofoil is still lacking in the literature.

The problem under consideration becomes more complicated for a cavitating hydrofoil. In addition to the unknown free surface, the cavity shape is also unknown and should be determined as part of the solution of the problem. Methods based on the complex-variable function theory effectively solve this kind of inverse boundary-value problem if the mathematical apparatus is based on the Christoffel–Schwartz and Schwartz integral formulae or the Sokhotsky–Plemel formula is applicable. These formulae provide the required analytical function (the complex potential or the complex conjugate velocity, or both) from its values on the real axis of the upper

half-plane (Dias & Vanden-Broeck 2003, 2004; Vanden-Broeck 2004; Chapman & Vanden-Broeck 2006).

A linear theory for a fully cavitating hydrofoil beneath the free surface, which is based on the Sokhotsky–Plemel formula and does not account for gravity effects, was presented by Tulin & Burkart (1955). Using the same mathematical technique, Larock & Street (1967*a*) presented nonlinear theories for a fully cavitating flat-plate beneath the free surface without gravity effects and for a fully cavitating flat-plate in an infinite fluid in the presence of a transverse gravity field (Larock & Street 1967*b*). Furuya (1975) extended the Larock & Street approach to predict characteristics of arbitrarily shaped supercavitating hydrofoils near the free surface without gravity effects. It is usually assumed that gravity effects for cavity flows are negligible. Taking into account that this assumption is valid for Froude numbers $Fn = V_\infty/\sqrt{gc}$ greater than 10 (Hough & Moran 1969), we obtain maximum chord size $c = V_\infty^2/(gFn^2) \approx 0.4\,\mathrm{m}$ for speed $V_\infty \approx 20\,\mathrm{m\,s^{-1}}$. The chord length of high-speed hydrofoils increases with the size of hydrofoil craft and may exceed this value. Besides, for supercavitating flows, the foil and cavity can be considered as a submerged body at zero angle of attack, whose length is much larger than the foil chord length. This means that gravity effects may affect the flow characteristics at typical Froude numbers.

In contrast to previous studies, here we present an exact nonlinear solution to the problem of the cavity flow past an arbitrarily shaped hydrofoil operating beneath the free surface in the presence of gravity. The proposed cavity closure scheme generalizes the Wu (1962) idea to simulate, in a certain sense, the cavity wake occurring in real flows and to obtain a single solution for both partial and fully developed cavitation. Besides, we obtain a solution for the cavity-free regime as a special case of the cavity-flow problem.

Our solution method follows that proposed by Zhukovskii (1890) for steady jet flows of an ideal fluid, the key step being the analytical construction of two governing functions: the complex velocity and the derivative of the complex potential defined in an auxiliary parameter region. The problem is formulated in § 2, where these governing functions are derived. The expression for the complex velocity depends on the variation of the velocity modulus along the free boundaries and the variation of the velocity angle along the wetted part of the foil. This function is given in terms of an auxiliary parameter variable, ζ, which lies in the first quadrant corresponding to the physical flow domain. By constructing the expression for the complex velocity, we have obtained a generalized integral formula making it possible to determine an analytical function from the values of its modulus and argument given on the boundary of a simply connected domain, which is applicable to different free-boundary flows. Some specific cases of this integral formula have already been obtained and used when solving the problems of a free-boundary flow in a corner-shaped Hele-Shaw cell (Semenov & Cummings 2006) and of self-similar asymmetric entry of a wedge into water (Semenov & Iafrati 2006).

For a given foil shape, we derive an integro-differential equation in the velocity angle along the foil and two integral equations in the velocity modulus. The first integral equation determines the velocity modulus along the cavity and the cavity closure streamlines, and the second determines the velocity modulus along the free surface of the flow. These integral equations must be solved numerically to complete the solution. In § 3, a method of successive approximations adopted for solving the integral equations is outlined.

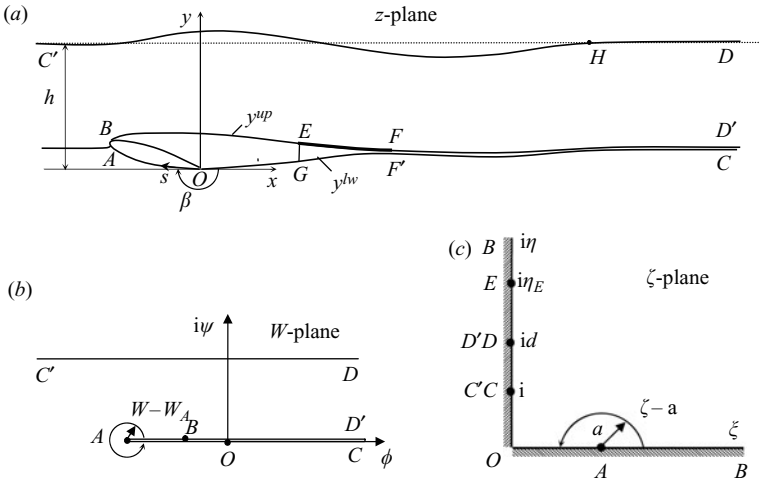

FIGURE 1. Sketch of the cavity flow past a hydrofoil beneath the free surface: (*a*) the physical plane; (*b*) the complex potential plane; (*c*) the parameter plane.

As a validation step, in § 4 careful comparisons are made between the calculated data and experimental data reported in the literature for the case of the cavity-free flow past a hydrofoil beneath the free surface. The results for cavity flows are reported in § 5 in terms of the force coefficients and cavity and free-surface shapes in a wide range of Froude numbers and depths of submergence.

2. Theoretical formulation and analysis

Figure 1(*a*) shows the flow configuration for our closed cavity-wake closure model. This model is similar to the Wu (1962) open cavity-wake model, and it simulates zero transverse pressure gradient in the wake downstream of the cavity. The shape of the foil is given by the angle β as a function of the spatial coordinate s along the foil, which starts at the trailing edge on the lower side. A flow parallel to the x-axis attacks the foil at incidence α. At the stagnation point A at the leading edge of the foil, the streamline splits into two streamlines, which go along the upper and lower sides of the foil. The first streamline detaches at some point B downstream of the stagnation point A. This streamline forms the upper cavity contour BE, which is closed by the curvilinear contour EF, whose shape is given as a one-parameter family of curves. The lower streamline starting at the stagnation point A detaches at the trailing point O of the foil and forms the lower cavity contour OG and the cavity closure contour GF'. Point F' coinciding with point F is achieved by choosing the form-parameter of the family of curves EF. The shape of the contour GF' is determined from the solution of the problem under the assumption that the transverse pressure gradient equals zero inside the cavity-wake region $EFF'G$. This assumption with the Bernoulli equation gives a relation between the velocity modulus along the upper, BEF, and lower, OGF', cavity and cavity closure contours.

The proposed flow scheme makes it possible to consider both partial and fully developed cavitation as specific cases of one and the same problem. The regimes of partial cavitation correspond to the case $x_E < x_O$. The other case corresponds to fully developed cavitation.

The Bernoulli equation can be written for two reference points: at upstream infinity at depth h or for the cavity detachment point B.

$$\rho\frac{V^2}{2}+\rho gY+p=\rho\frac{V_\infty^2}{2}+\rho gh+p_a=\rho\frac{V_B^2}{2}+\rho gY_B+p_c, \tag{2.1}$$

where ρ is the liquid density; g is the acceleration due to gravity; p_a is the atmospheric pressure; h is the depth of submergence relative to the trailing edge of the foil; V_∞ and V_B are the inflow velocity and the velocity at the cavity detachment point; p_c is the pressure in the cavity and Y_B is the y-coordinate of the cavity detachment point. The reference elevation is chosen to be zero at the trailing edge of the foil (point O).

Two dimensionless quantities are obtained from (2.1): the cavitation number σ and the Froude number,

$$\sigma=\frac{p_\infty-p_c}{\frac{1}{2}\rho V_\infty^2},\quad Fn=\frac{V_\infty}{\sqrt{gc}},\quad p_\infty=p_a+\rho gh. \tag{2.2}$$

Using the chord length c as the characteristic dimension and the inflow velocity V_∞ as the characteristic velocity, (2.1) takes the form

$$v^2=1-c_p-\frac{2y}{Fn^2},\quad c_p=\frac{p-p_\infty}{\frac{1}{2}\rho V_\infty^2}, \tag{2.3}$$

where $v=V/V_\infty$ and $y=Y/c$ are the dimensionless velocity and coordinate, respectively. Equation (2.3) determines the velocity modulus along the cavity boundaries where $c_p=-\sigma$ and along the free surface where $c_p=-2(h/c)/Fn^2$.

The flow region past the hydrofoil beneath the free surface is a doubly connected domain. This means that the flow potential can be expressed only by using doubly periodic elliptic functions of complex variable. In order to avoid the computation of elliptic functions, we continue the closing contour EF to infinity and consider the upper, FD', and lower, $F'C$, sides of the streamline as independent lines. The obtained flow region becomes a simply connected domain. The same shape of the lines FD' and $F'C$ and the same velocity distribution are the conditions for the determination of the velocity modulus along the contours FD' and $F'C$ as independent lines.

According to the Helmholtz (1868) and Kirchoff (1869) method, the problem is to find a function that conformally maps the flow region in the physical plane z onto the complex potential plane W. Then, the velocity field is determined by the derivative of the complex potential,

$$v_x-\mathrm{i}v_y=\frac{\mathrm{d}W}{\mathrm{d}z},$$

where v_x and v_y are the x and y velocity components.

Usually, finding the function $W=W(z)$ directly is a complicated problem. Instead, Zhukovskii (1890) proposed to map the upper half-plane onto the planes of two functions, which are the complex potential W and the function $\omega=-\ln(\mathrm{d}W/\mathrm{d}z)$. For steady jet flows past polygonal bodies, the map of the fluid region onto the W-plane and the ω-plane has polygonal shapes, and the mapping function can be found using the Schwartz–Christoffel formula. If $W(\zeta)$ and $\omega(\zeta)$ are known functions of the parameter variable ζ, the velocity field and the function mapping the parameter plane onto the physical plane can be determined as follows:

$$\frac{\mathrm{d}W}{\mathrm{d}z}=\exp\left[-\omega(\zeta)\right],\quad z(\zeta)=z_0+\int_0^\zeta\frac{\mathrm{d}W/\mathrm{d}\zeta'}{\mathrm{d}W/\mathrm{d}z}\,\mathrm{d}\zeta'. \tag{2.4}$$

In contrast to steady flows of a weightless fluid past polygonal-shaped bodies, for the problem under consideration, the velocity modulus varies along the free surface and the argument of the velocity changes along the foil; therefore, we have to use a different way of constructing expressions for the complex velocity $\mathrm{d}W/\mathrm{d}z$ and for the derivative of the complex potential $\mathrm{d}W/\mathrm{d}\zeta$.

We choose the first quadrant of the ζ-plane, where the complex variable $\zeta = \xi + \mathrm{i}\eta$ (figure 1*c*), to correspond to the physical plane. A conformal mapping allows us to fix three points O, B and C as shown in figure 1(*c*), then $\zeta = a$ and $\zeta = \mathrm{i}d$ are the images of points A and D in the physical plane, which should be determined from additional conditions. The interval $0 < \eta < 1$ of the imaginary axis corresponds to the lower free boundary $OGF'C$, the interval $1 < \eta < d$ corresponds to the free surface $C'D$, and the interval $d < \eta < \infty$ corresponds to the upper free boundary $D'FEB$. The real axis $0 < \xi < \infty$ corresponds to the wetted part OAB of the foil. Since the actual range of the complex velocity is unknown *a priori*, an explicit conformal transformation of the first quadrant onto the complex velocity plane is a complicated problem.

2.1. *Expressions for the complex velocity and for the derivative of the complex potential*

At this stage, we assume that the modulus of the complex velocity is known on the free boundaries as a function of the parameter variable η and its argument is known on the wetted part of the hydrofoil as a function of the parameter variable ξ, i.e. the function $\mathrm{d}W/\mathrm{d}z$ satisfies the following boundary conditions

$$\left|\frac{\mathrm{d}W}{\mathrm{d}z}\right|_{\zeta=\mathrm{i}\eta} = v(\eta), \quad 0 < \eta < \infty, \tag{2.5}$$

$$\arg\left(\frac{\mathrm{d}W}{\mathrm{d}z}\right)\Bigg|_{\zeta=\xi} = \begin{cases} -\pi - \beta, & 0 < \xi < a, \\ -\beta, & a < \xi < \infty, \end{cases} \tag{2.6}$$

where β is the slope of the wetted part of the hydrofoil. The argument of the complex velocity undergoes a step change at the point $\zeta = a$ corresponding to the splitting of the streamline at the stagnation point A in the physical plane.

By using the mathematical technique based on Chaplygin's singular-point method (Semenov & Iafrati 2006) or applying the more refined mathematical apparatus (Semenov & Cummings 2006), it is possible to determine an analytical function from its modulus and argument given on the imaginary and real axes of the first quadrant. By following this technique, the final expression for the complex velocity takes the form

$$\frac{\mathrm{d}W}{\mathrm{d}z} = v_0\left(\frac{\zeta - a}{\zeta + a}\right)\exp\left[-\frac{1}{\pi}\int_0^\infty \frac{\mathrm{d}\beta}{\mathrm{d}\xi'}\ln\left(\frac{\zeta + \xi'}{\zeta - \xi'}\right)\mathrm{d}\xi' - \frac{\mathrm{i}}{\pi}\int_0^\infty \frac{\mathrm{d}\ln v}{\mathrm{d}\eta'}\ln\left(\frac{\mathrm{i}\eta' - \zeta}{\mathrm{i}\eta' + \zeta}\right)\mathrm{d}\eta' - \mathrm{i}\beta_B\right]. \tag{2.7}$$

It is easy to see that (2.7) satisfies the boundary conditions (2.5) and (2.6). Setting $\zeta = \xi$ in (2.7), it can be seen that $\arg(\mathrm{d}W/\mathrm{d}z) = -\beta(\xi)$ for $\xi > a$ and $\arg(\mathrm{d}W/\mathrm{d}z) = -\pi - \beta(\xi)$ for $0 < \xi < a$, i.e. (2.7) satisfies the boundary condition (2.6). On the free boundaries ($\zeta = \mathrm{i}\eta$), the modulus of (2.7) equals the given function $v(\eta)$.

For steady free-boundary flows, the streamfunction $\psi(x, y)$ takes a constant value along the body and free boundaries, therefore the region boundary in the W-plane

forms a polygonal region (figure 1*b*). According to Chaplygin's singular point method (Gurevich 1965), to determine the function $W = W(\zeta)$, it is sufficient to analyse all singular points where the mapping is not conformal. The function $W = W(\zeta)$ has singularities at points O ($\zeta = 0$), A ($\zeta = a$), C ($\zeta = \mathrm{i}$), and D ($\zeta = \mathrm{i}d$), which correspond to the corner points of the region boundary in the ζ-plane and the W-plane. The analysis of the behavior of the function $\arg(W)$ at each corner point makes it possible to determine the order of the singularities in the expression $W = W(\zeta)$, whose differentiation yields

$$\frac{\mathrm{d}W}{\mathrm{d}\zeta} = K\frac{\zeta(\zeta^2 - a^2)}{(\zeta^2+1)^2(\zeta^2+d^2)}, \tag{2.8}$$

where K is a real scale factor.

Dividing (2.8) by (2.7), we obtain the derivative of the mapping function

$$\frac{\mathrm{d}z}{\mathrm{d}\zeta} = \frac{K}{v_0}\frac{\zeta(\zeta+a)^2}{(\zeta^2+1)^2(\zeta^2+d^2)}\exp\left[\frac{1}{\pi}\int_0^\infty \frac{\mathrm{d}\beta}{\mathrm{d}\xi'}\ln\left(\frac{\zeta+\xi'}{\zeta-\xi'}\right)\mathrm{d}\xi' + \frac{\mathrm{i}}{\pi}\int_0^\infty \frac{\mathrm{d}\ln v}{\mathrm{d}\eta'}\ln\left(\frac{\zeta-\mathrm{i}\eta'}{\zeta+\mathrm{i}\eta'}\right)\mathrm{d}\eta' + \mathrm{i}\beta_B\right], \tag{2.9}$$

whose integration along the imaginary axis in the parameter region provides the free boundaries $OGF'C$ and $BEFD'$ and the free surface $C'D$ in the z-plane. The parameters a, d, K and the functions $v(\eta)$ and $\beta(\xi)$ are determined from the boundary conditions and from physical considerations.

At infinity, the inflow velocity approaches the value v_∞ directed along the x-axis. By taking the argument of the complex velocity (2.7) when $\zeta = \mathrm{i}$ we obtain the following nonlinear equation

$$\frac{1}{\pi}\int_0^\infty \frac{\mathrm{d}\ln v}{\mathrm{d}\eta}\ln\left|\frac{\eta-1}{\eta+1}\right|\mathrm{d}\eta + 2\arctan\left(\frac{1}{a}\right) + \frac{2}{\pi}\int_0^\infty \frac{\mathrm{d}\beta}{\mathrm{d}\xi}\arctan\left(\frac{1}{\xi}\right)\mathrm{d}\xi + \beta(0) - \pi = 0. \tag{2.10}$$

The depth of submergence h is determined by integrating (2.9) over the interval $0 < \eta < 1$, which corresponds to going along the lower boundary OC and around the point $\zeta = \mathrm{i}$. The latter corresponds to going in a clockwise direction along a large-radius curve in the physical plane, i.e.

$$h = \mathrm{Im}\left(\int_0^1 \left.\frac{\mathrm{d}z}{\mathrm{d}\zeta}\right|_{\zeta=\mathrm{i}\eta}\mathrm{i}\mathrm{d}\eta + \oint_{\zeta=\mathrm{i}}\frac{\mathrm{d}z}{\mathrm{d}\zeta}\mathrm{d}\zeta\right) = \mathrm{Im}\left(\int_0^1 \left.\frac{\mathrm{d}z}{\mathrm{d}\zeta}\right|_{\zeta=\mathrm{i}\eta}\mathrm{i}\mathrm{d}\eta\right) + \psi_0 c, \tag{2.11}$$

where the second integral is evaluated by the residue method;

$$\psi_0 = \frac{\pi K}{2}\frac{a^2+d^2}{(d^2-1)^2}$$

is the flow rate in the channel formed by the lines $BEFD'$ and free surface $C'D$. The parameter ψ_0 can be considered as the flow parameter instead of the depth of submergence h. The residue integration assumes that the part of the free surface HD extending to infinity is parallel to the x-axis.

At this stage, we assume that the cavity detaches at some point B at the leading edge and the length S_w of the wetted part of the hydrofoil is known. Hence, by

integrating the expression $\mathrm{d}s/\mathrm{d}\xi = |\mathrm{d}z/\mathrm{d}\zeta|_{\zeta=\xi}$ along the real axis $0 < \xi < \infty$, we have

$$\int_0^\infty \frac{\mathrm{d}s}{\mathrm{d}\xi}\mathrm{d}\xi = S_w, \tag{2.12}$$

where

$$\frac{\mathrm{d}s}{\mathrm{d}\xi} = \frac{K}{v_0}\frac{\xi(\xi+a)^2}{(\xi^2+1)^2(\xi^2+d^2)}\exp\left[\frac{1}{\pi}\int_0^\infty \frac{\mathrm{d}\beta}{\mathrm{d}\xi'}\ln\left|\frac{\xi+\xi'}{\xi-\xi'}\right|\mathrm{d}\xi' + \frac{2}{\pi}\int_0^\infty \frac{\mathrm{d}\ln v}{\mathrm{d}\eta'}\arctan\frac{\eta'}{\xi}\mathrm{d}\eta'\right]. \tag{2.13}$$

Equations (2.10)–(2.12) allow us to determine the unknown parameters a, d and K, once the functions $v(\eta)$ and $\beta(\xi)$ are specified.

2.2. *System of integro-differential equations*

By integrating (2.13) along the real axis of the parameter region, we can determine the spatial coordinate along the foil as a function of the parameter variable

$$s(\xi) = \int_0^\xi \mathrm{d}s/\mathrm{d}\xi\ \mathrm{d}\xi.$$

Since the function $\beta = \beta(s)$ is known, the function $\beta(\xi)$ is determined from the following integro-differential equation

$$\frac{\mathrm{d}\beta}{\mathrm{d}\xi} = \frac{\mathrm{d}\beta}{\mathrm{d}s}\frac{\mathrm{d}s}{\mathrm{d}\xi};$$

by substituting $\mathrm{d}s/\mathrm{d}\xi$ from (2.13), this equation takes the form

$$\frac{\mathrm{d}\beta}{\mathrm{d}\xi} = \frac{K}{v_0}\frac{\chi[s(\xi)]\xi(\xi+a)^2}{(\xi^2+1)^2(\xi^2+d^2)}\exp\left[\frac{1}{\pi}\int_0^\infty \frac{\mathrm{d}\beta}{\mathrm{d}\xi'}\ln\left|\frac{\xi+\xi'}{\xi-\xi'}\right|\mathrm{d}\xi' + \frac{2}{\pi}\int_0^\infty \frac{\mathrm{d}\ln v}{\mathrm{d}\eta'}\arctan\frac{\eta'}{\xi}\mathrm{d}\eta'\right], \tag{2.14}$$

where $\chi(s) = \mathrm{d}\beta/\mathrm{d}s$ is the foil curvature.

Cavity closure model and the corresponding integral equation

The velocity modulus function $v(\eta)$ on the interval (η_E, ∞) on the imaginary axis of the parameter region, which corresponds to the upper cavity contour EB, is determined by (2.3). In order to determine the velocity modulus on the interval (d, η_E), which corresponds to the contour $D'FE$, we first determine the slope of the contour EF as a one-parameter family of circular arcs

$$\beta^{up}(x) = \beta_E + (\beta_F - \beta_E)\frac{x - x_E}{L_c}. \tag{2.15}$$

Here, x_E is the x-coordinate of point E, $L_c = x_F - x_E$ is the given x-projection of the contour EF, $\beta_F = \arctan(\mathrm{d}y^{lw}/\mathrm{d}x)|_{x=x_F}$ is the slope of the lower contour $GF'C$ at point F. The free parameter β_E, which is the slope of the cavity contour BE at point E, is determined from the conditions

$$y^{up}(x_F) = y^{lw}(x'_F), \quad x_F = x'_F, \tag{2.16}$$

which means the coincidence of points F and F' lying on the upper and lower cavity closure contours. The upper and lower boundaries are determined by integration of the derivative of the mapping function (2.9)

$$x^{up}(\eta) = \mathrm{Re}[z^{up}(\eta)], \quad y^{up}(\eta) = \mathrm{Im}[z^{up}(\eta)], \quad z^{up}(\eta) = z_B + \int_\infty^{\mathrm{i}\eta} \left.\frac{\mathrm{d}z}{\mathrm{d}\zeta}\right|_{\zeta=\mathrm{i}\eta'} \mathrm{i}\mathrm{d}\eta', \tag{2.17}$$

$$x^{lw}(\eta) = \mathrm{Re}[z^{lw}(\eta)], \quad y^{lw}(\eta) = \mathrm{Im}[z^{lw}(\eta)], \quad z^{lw}(\eta) = \int_0^{i\eta} \left.\frac{\mathrm{d}z}{\mathrm{d}\zeta}\right|_{\zeta=i\eta'} i\mathrm{d}\eta'. \tag{2.18}$$

By starting from the point F the upper contour FD' is congruent to the lower contour $F'C$, i.e.

$$\beta^{up}[x(\eta)] = \arctan\left\{\frac{\mathrm{d}y^{lw}}{\mathrm{d}x}(x)\right\} = -\arg\left(\left.\frac{\mathrm{d}W}{\mathrm{d}z}\right|_{\zeta=i\eta}\right), \quad d < \eta < \eta_F. \tag{2.19}$$

By taking the argument of the complex velocity in expression (2.7) when $\zeta = i\eta$, the following integral equation respect to the function $d(\ln v)/\mathrm{d}\eta$ is obtained

$$\frac{1}{\pi}\int_d^{\eta_E} \frac{\mathrm{d}\ln v}{\mathrm{d}\eta'} \ln\left|\frac{\eta'-\eta}{\eta'+\eta}\right| \mathrm{d}\eta' = R(\eta), \quad d < \eta < \eta_E, \tag{2.20}$$

where

$$R(\eta) = \beta^{up}[x(\eta)] - \left\{\int_0^d + \int_{\eta_E}^{\infty}\right\} \frac{\mathrm{d}\ln v}{\mathrm{d}\eta'} \ln\left|\frac{\eta'-\eta}{\eta'+\eta}\right| \mathrm{d}\eta' - \frac{2}{\pi}\int_0^{\infty} \frac{\mathrm{d}\beta}{\mathrm{d}\xi} \arctan\left(\frac{\eta}{\xi}\right)\mathrm{d}\xi$$

$$-2\arctan\left(\frac{\eta}{a}\right) + \pi - \beta(0),$$

On the interval $0 < \eta < 1$ corresponding to the lower boundary OC, the function $v(\eta) = v^{lw}[x^{lw}(\eta)]$ is determined according to the cavity closure model, which provides zero transverse pressure gradient in the cavity closure region $EFF'G$. From the Bernoulli equation

$$(v^{lw})^2 = \begin{cases} (v^{up})^2 + \dfrac{2}{Fn^2}(y^{up} - y^{lw}), & 0 < x < x_{F'}, \\ (v^{up})^2, & x_{F'} < x < \infty, \end{cases} \tag{2.21}$$

where

$$v^{up}[x^{up}(\eta)] = v_B \exp\left(\int_{\infty}^{\eta} \frac{\mathrm{d}\ln v}{\mathrm{d}\eta'}\mathrm{d}\eta'\right), \quad d < \eta < \infty.$$

Equation (2.21) provides the same velocity on the lower, $F'C$, and upper, FD', sides of one and the same streamline. The expression for the function $R(\eta)$ includes the unknown function $\mathrm{d}(\ln v)/\mathrm{d}\eta$ on the interval $1 < \eta < d$ corresponding to the free surface $C'D$, which is determined from the boundary condition on the free surface.

Free-surface boundary condition

Differentiating with respect to the spatial coordinate the Bernoulli equation (2.3) written for the free surface, we obtain

$$v\frac{\mathrm{d}v}{\mathrm{d}s} + \frac{1}{Fn^2}\sin\beta^{fr} = 0, \tag{2.22}$$

where $\sin\beta^{fr} = \mathrm{d}y/\mathrm{d}s$ is the velocity direction on the free surface determined by the expression for the complex velocity. Taking the argument of (2.7) when $\zeta = i\eta$, we obtain

$$\beta^{fr}(\eta) = \frac{2}{\pi}\int_0^{\infty} \frac{\mathrm{d}\beta}{\mathrm{d}\xi'} \arctan\frac{\eta}{\xi'}\mathrm{d}\xi' + \frac{1}{\pi}\int_0^{\infty} \frac{\mathrm{d}\ln v}{\mathrm{d}\eta'} \ln\left|\frac{\eta'-\eta}{\eta'-\eta}\right| \mathrm{d}\eta' + 2\arctan\frac{\eta}{a} + \pi - \beta_0. \tag{2.23}$$

Using the relations

$$\frac{\mathrm{d}v}{\mathrm{d}s} = v\frac{\mathrm{d}\ln v}{\mathrm{d}\eta}\Big/\frac{\mathrm{d}s}{\mathrm{d}\eta},$$

and

$$\frac{\mathrm{d}s}{\mathrm{d}\eta} = \left|\frac{\mathrm{d}z}{\mathrm{d}\zeta}\right|_{\zeta=\mathrm{i}\eta} = \frac{1}{v}\left|\frac{\mathrm{d}W}{\mathrm{d}\zeta}\right|_{\zeta=\mathrm{i}\eta} = \frac{K}{v(\eta)}\frac{\eta(\eta^2+a^2)}{(1-\eta^2)^2(d^2-\eta^2)},$$

we can recast the boundary condition (2.22) as the following integral equation in the function $\mathrm{d}(\ln v)/\mathrm{d}\eta$ on the interval $1 < \eta < d$

$$Fn^2v^3\frac{\mathrm{d}\ln v}{\mathrm{d}\eta} + K\frac{\eta(\eta^2+a^2)}{(1-\eta^2)^2(d^2-\eta^2)}\sin\left[\frac{1}{\pi}\int_1^d \frac{\mathrm{d}\ln v}{\mathrm{d}\eta'}\ln\left|\frac{\eta'-\eta}{\eta'-\eta}\right|\mathrm{d}\eta' + P(\eta)\right] = 0, \tag{2.24}$$

where

$$P(\eta) = \left\{\int_0^1 + \int_d^\infty\right\}\frac{\mathrm{d}\ln v}{\mathrm{d}\eta'}\ln\left|\frac{\eta'-\eta}{\eta'+\eta}\right|\mathrm{d}\eta' + \frac{2}{\pi}\int_0^\infty \frac{\mathrm{d}\beta}{\mathrm{d}\xi}\arctan\left(\frac{\eta}{\xi}\right)\mathrm{d}\xi$$
$$+2\arctan\left(\frac{\eta}{a}\right) + \pi - \beta(0),$$
$$v(\eta) = v_\infty\exp\left(\int_1^\eta \frac{\mathrm{d}\ln v}{\mathrm{d}\eta'}\mathrm{d}\eta'\right).$$

The velocity modulus function $v(\eta)$ is determined by (2.3) and (2.21) and the integral equations (2.20) and (2.24) on the whole imaginary axis of the parameter region, while the function $\beta(\xi)$ is determined by the integral equation (2.14) on the whole real axis.

2.3. *Cavity detachment*

For foils with a sharp leading edge, the cavity detachment point is fixed, and thus the length of the wetted part of the foil, S_w, is known. For smoothly shaped hydrofoils, the cavity detachment position is unknown and should be determined from an additional condition. In the model of ideal fluid, this condition is well known as the Brillouin–Villat criterion. It is also well known (Arakeri 1975) that in real flows, laminar separation occurs before cavity detachment and delays cavity formation. In this case, the pressure increases downstream from the laminar separation point to the cavity detachment. Therefore, there is a point where the pressure goes through a minimum, which is lower than the pressure in the cavity. For further details, see Smith (1986).

For various theories of cavity detachment, the Brillouin–Villat criterion remains the condition that predicts the position of the minimum pressure on the foil, which is also true for the viscous/inviscid interaction model of cavity flow. In terms of the present study, it is point B that is both the minimum pressure point and the cavity detachment point. In terms of the velocity modulus along the foil, the Brillouin–Villat criterion takes the form

$$\lim_{s\to S_w}\frac{\mathrm{d}\ln v}{\mathrm{d}s} = 0. \tag{2.25}$$

Using the relation

$$\frac{\mathrm{d}\ln v}{\mathrm{d}s} = \frac{\mathrm{d}\ln v}{\mathrm{d}\xi}\Big/\frac{\mathrm{d}s}{\mathrm{d}\xi},$$

differentiating the function $v(\xi) = |\mathrm{d}W/\mathrm{d}z|_{\zeta=\xi}$ and substituting the result into (2.25), we obtain

$$\int_0^\infty \frac{\mathrm{d}\ln v}{\mathrm{d}\eta'}\eta'\mathrm{d}\eta' + \int_0^\infty \frac{\mathrm{d}\beta}{\mathrm{d}\xi'}\xi'\mathrm{d}\xi' + \pi a = 0. \tag{2.26}$$

This is an equation in the unknown length of the wetted part of the foil, S_w, which affects the function $\beta(\xi) = \beta[s(\xi)]$, $0 < s < S_w$.

2.4. *Force coefficients*

The drag D and lift L are evaluated by integrating the pressure along the closed foil surface Γ in a clockwise direction

$$F_D + \mathrm{i}F_L = -\mathrm{i}c \oint_\Gamma (p - p_\infty)\,\mathrm{d}z, \tag{2.27}$$

where c is the chord length of the foil, the pressure $p = p_c$ along the foil surface occupied by the cavity, $x_B \leqslant x \leqslant x_E$, and $p = p_w(x)$ along the foil, $x_E \leqslant x \leqslant 0$, where the cavity closure contour EF may occur for the regime of partial cavitation, i.e. when $x_E \leqslant 0$; $p_w(x)$ is the pressure along the contour EF.

Defining the drag and lift coefficients, respectively, as

$$C_D = \frac{F_D}{\frac{1}{2}\rho\, v_\infty^2 c}, \quad C_L = \frac{F_L}{\frac{1}{2}\rho\, v_\infty^2 c}, \tag{2.28}$$

we obtain the following expression

$$C_D + \mathrm{i}C_L = -\mathrm{i}\oint_\Gamma \left(1 - v^2 - \frac{2y}{Fn^2}\right)\mathrm{d}z = \mathrm{i}\oint_\Gamma v^2\mathrm{d}z + \mathrm{i}\frac{2A}{Fn^2}, \tag{2.29}$$

where $v[x(\xi), y(\xi)] = |\mathrm{d}W/\mathrm{d}z|_{\zeta=\xi}$ is the velocity modulus along the wetted part of the hydrofoil and $v[x^{up}(\eta), y^{up}(\eta)] = v(\eta)$ along the cavity side of the foil, A is the foil cross-sectional area. The second term represents the buoyancy force due to gravity for cavitation-free regimes, and it affects only the lift coefficient.

3. Numerical method and its validation

3.1. *Numerical approach*

In discrete form, the solution is sought on a fixed set of points ξ_i, $i = 1, \ldots, N$ distributed along the real axis of the parameter region and a fixed set of points η_j, $j = 1, \ldots, M$ distributed along the imaginary axis. The total number of points ξ_i was chosen in the range $N = 200$–400, and the total number of points η_j was chosen in the range $M = 500$–1500 to check convergence of the solution procedure. For all calculated examples, the difference between the results for the above ranges of N and M is within the last three figures only.

The points ξ_i are distributed so as to provide a higher density of the points $s_i = s(\xi_i)$ at the leading edge of the foil, where the slope $\beta(s)$ changes rapidly and the stagnation point occurs. The distribution of the points η_j is chosen so as to provide a higher density of the points $s_j = s(\eta_j)$ on the free boundaries closer to the foil.

The integrals occurring in the system of equations are evaluated using the linear interpolation of the functions $\beta(\xi)$ and $\ln v(\eta)$ on the intervals (ξ_{i-1}, ξ_i) and (η_{j-1}, η_j), respectively. Besides, because of the logarithmic singularity of the complex potential at point D, the integrals along the imaginary axis were evaluated through the variable

$$p = \ln|\eta - d|, \tag{3.1}$$

which makes it possible to take into consideration a flow region downstream of the foil large enough to include at least three crests of the wave surface.

The integral equations (2.14), (2.20) and (2.24) were solved using the method of successive approximations. The iteration procedure is as follows.

1. In the first iteration, the functions $\beta(\xi)$ and $v(\eta)$ are given as $\beta(\xi) \equiv \beta(0)$ and $v(\eta) \equiv v_\infty$ to find the solution of the system of nonlinear equations (2.10)–(2.12).

2. The integro-differential equation (2.14) is solved by internal iteration including the system of nonlinear equations (2.10)–(2.12). The result is the computed function $\beta(\xi)$.

3. The integral equation (2.20) is solved by internal iteration including the system of nonlinear equations (2.10)–(2.12) and using the conditions (2.15), (2.19) and (2.21). The result is the velocity modulus function computed along the upper and lower cavity boundaries and closure contours continuing downstream as congruent streamlines.

4. The iteration process is repeated starting from step 2 until convergence is reached. The solution obtained in the first external iteration corresponds to the cavity flow of a weightless fluid.

5. By solving the integral equation (2.24), a new velocity modulus function $v(\eta)$ along the free surface is determined. The next external iteration starts from step 2.

3.2. *Validation of the numerical approach for a fully cavitating flat plate without gravity*

For validation purposes, the numerical approach is applied to solve the cavity flow past a flat plate beneath the free surface of a weightless fluid. This problem is much simpler since the function $\beta(\xi) \equiv \alpha - \pi$ and the velocity modulus on the free surface $v(\eta) \equiv v_\infty$, $1 < \eta < d$. Only one nonlinear integral equation, (2.20), together with equations (2.15), (2.19) and (2.21) has to be solved for the determination of the velocity modulus along the upper and lower cavity and closure contours.

In figure 2, the lift coefficient divided by α as a function of the streamfunction on the free surface is shown and compared with the Larock & Street (1967*a*) nonlinear solution for a fully cavitating flat plate beneath the free surface. Larock & Street (1967*b*) used a 'double-spiral-vortex' model (Tulin's second scheme) for the cavity closure and formulated a mixed-boundary-value problem for the complex velocity function, whose solution is based on the Sokhotsky–Plemel formula. The discrepancy between the obtained and Larock & Street (1967*a*) results is less than 5% for depths of submergence $h \approx \psi_0/v_\infty > 1$. However, for lower depths and angles of attack $\alpha > 7^0$, Larock & Street's results do not agree with the present solution, and there are no physical causes for lift reduction as the foil approaches the free surface. On the contrary, the hill on the free surface over the cavity becomes larger. This increases the local angle of attack near the foil and, correspondingly, the lift force. Besides, the linear theory by Johnson (1961) predicts a lift increase up to the value $C_L/\alpha = \pi$ when $\psi_0 \to 0$. The difference in the ratio C_L/α for different angles of attack shows the nonlinear effects of the solutions.

3.3. *Validation for non-cavitating flows under the action of gravity*

The next step in validating the numerical procedure involves all the derived integral equations. In order to consider the cavity-free regime as a specific case of the solution derived in § 2, we put the cavity length equal to zero and consider the upper side of the foil ET as a part of the cavity closure contour EF (figure 3). The part TF is given

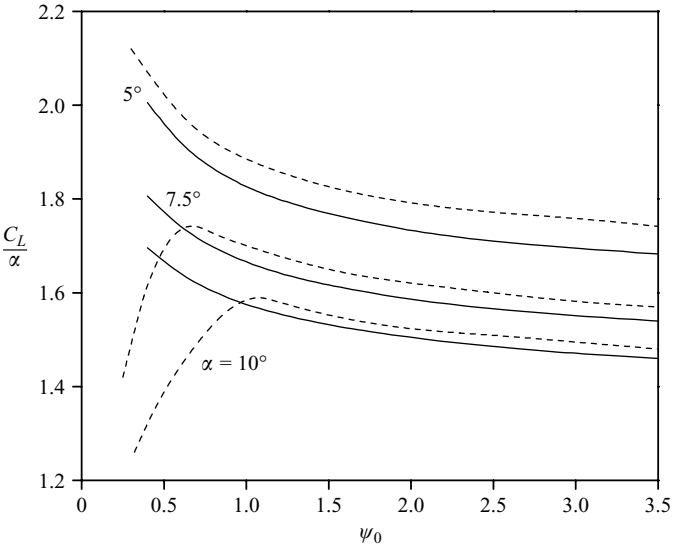

FIGURE 2. Comparison between the present (solid lines) and Larock & Street (1967*a*) (dashed lines) solution for the lift coefficient divided by α as a function of the streamfunction on the free surface at cavitation number $\sigma = 0.075$.

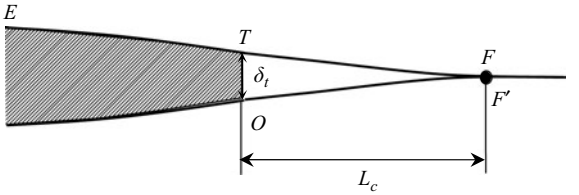

FIGURE 3. Model of flow around the trailing edge of NACA hydrofoils of thickness δ_t.

by the slightly modified (2.15)

$$\beta^{up}(x) = \beta_T + (\beta_F - \beta_T)\frac{x - x_T}{L_c}, \quad x_T < x < x_T + L_c, \tag{3.2}$$

where β_T is the foil slope at the trailing edge of the foil (point T) and the length L_c is chosen to satisfy the condition (2.16).

There is some arbitrariness in the placement of point E. It might be chosen directly at the trailing edge of the foil. However, in this case for low depths of submergence, $h/c < 1$, the parameters a, d, K become too large owing to the logarithmic singularity in the complex potential at point D. In physical terms, this means a weak interference of the flow parameters on the lower and upper sides of the hydrofoil for low depths of submergence. If point E is chosen close to the leading edge of the foil, then the flow region between the upper side of the foil and the free surface belongs to the channel formed by the free streamlines $BEFD'$ and $C'D$. This region corresponds to a very small vicinity, $|\varsigma - \mathrm{i}d| < \varepsilon$, of point D in the parameter plane and, therefore, affects the parameters a, d and K only slightly. The interaction between the main and the channel flow downstream of the foil is provided in the physical plane owing to the conditions (2.16), (2.19) and (2.21) enforcing the same shape and velocity along the streamlines FD' and $F'C$.

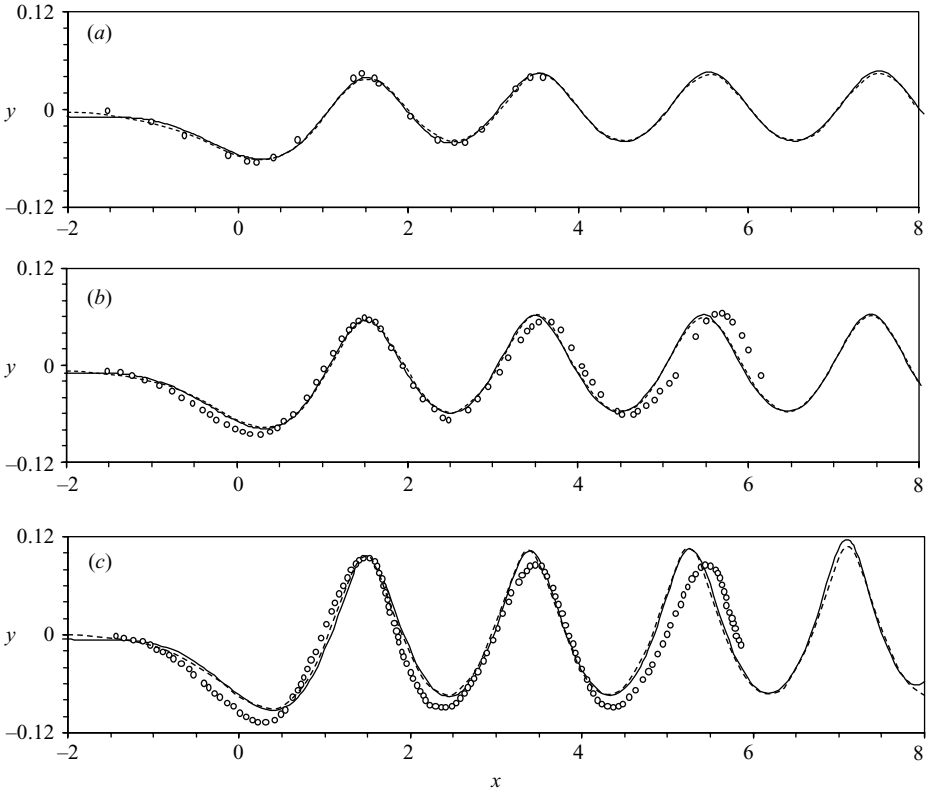

FIGURE 4. Wave height past the NACA 0012 at incidence $\alpha = 5^\circ$ and $Fn = 0.5669$ for depth of submergence (*a*) $h/c = 1.286$, (*b*) $h/c = 1.163$, (*c*) $h/c = 1.035$ measured from the mid-chord point. Solid lines, present solution; dashed lines, Landrini *et al.* (1999) fully nonlinear numerical approach; ○, measurements from Duncan (1983).

The free-surface elevations for the flow past the NACA 0012 hydrofoil at angle of attack $\alpha = 5^\circ$ and Froude number $Fn = 0.5669$ are shown in figure 4 and compared with experimental data (Duncan 1983) and with the results obtained through the fully nonlinear numerical approach by Landrini, Lugni & Bertram (1999). Agreement with the fully nonlinear numerical model is reasonably good. The discrepancy between the experimental and calculated data for a lower depth of submergence (figure 4*c*) also occurs for other numerical approaches as shown by Landrini *et al.* (see references therein).

Another validation step is made by considering the shape of the free surface downstream. In figure 5, the wave profiles downstream of the NACA 0012 hydrofoil at angle of attack $\alpha = 3^\circ$, Froude number $Fn = 0.7$ and several depths of submergence are shown and compared with the numerical solution for progressive wave motion (M. Greco 2006, personal communication). This figure also shows analytical results of Schwartz (1974) for the second-order approximation of the Stokes progressive free-surface wave profiles. Agreement with the fully nonlinear numerical solution is rather fine (the difference is invisible) while the second-order Stokes theory predicts a somewhat smaller wave steepness. The depths of submergence and the corresponding wavelengths and heights are presented in table 1. The length of progressive waves predicted by the linear theory for Froude number $Fn = 0.7$ is $\lambda_{lin}/c = 2\pi Fn^2 = 3.08$. As shown in table 1, the nonlinear effects slightly reduce the wavelength.

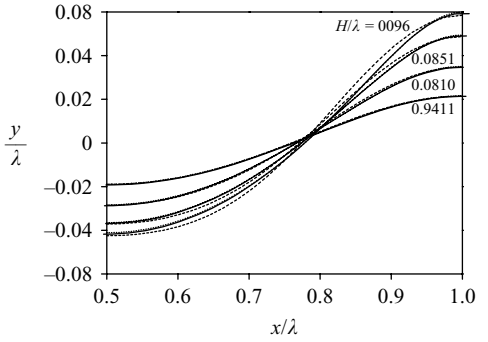

FIGURE 5. Wave profiles downstream of the NACA 0012 hydrofoil at angle of attack $\alpha = 3^\circ$ and Froude number $Fn = 0.7$ for several depths of submergence shown in table 1. Solid lines, present solution; dashed lines, second-order Stokes theory; dotted lines, Greco's fully nonlinear numerical solver.

h/c	λ	$\lambda/\lambda_{lin,}$%	H/c	H/λ
0.840	2.810	91.3	0.280	0.0996
0.940	2.880	93.5	0.245	0.0851
1.129	2.985	97.0	0.182	0.0610
1.330	3.045	98.9	0.125	0.0411

TABLE 1. Length and height of the wave downstream of the NACA 0012 hydrofoil at angle of attack $\alpha = 3^\circ$ and Froude number $Fn = 0.7$ with several depths of submergence.

The verification of the numerical results concerning the force coefficients is based on comparison with the results predicted by linear theories. Kochin (1937) gave a solution for the flow around a submerged vortex with a linearized free-surface boundary condition and derived the formula

$$C_D/C_L^2 = 0.5/Fn\ \exp[-2/Fn_h]. \tag{3.3}$$

Because the lift force arises from the velocity circulation around the hydrofoil, this formula is applicable to evaluating the wave-drag force for thin submerged hydrofoils if the velocity circulation is known.

In figure 6, the ratio C_D/C_L^2 is shown as a function of the submergence Froude number for the NACA 0012 hydrofoil at an angle of attack of 3° for various depths of submergence (dashed lines). Agreement between the nonlinear solution and the dependence (3.3) is reasonably good. This means a minor contribution of the nonlinear effects on the free surface to the force coefficients. Some difference occurs at the maximum of the dependencies corresponding to the maximum of the wave steepness on the free surface downstream of the hydrofoil. The obtained agreement also shows a weak influence of the NACA 0012 hydrofoil thickness.

Hough & Moran (1969) obtained a linear solution for the flow past a thin submerged hydrofoil in the presence of gravity and identified the lift reduction due to gravity. Their results are presented in terms of the ratio $C_L/C^*_{L\,inf}$, where $C^*_{L\,inf}$ is the lift coefficient at infinite depth. For a thick hydrofoil like the NACA 0012, the lift $C_{L\,inf}(Fn) = C^*_{L\,inf} + 2A/Fn^2$ includes both the hydrodynamic lift $C^*_{L\,inf}$ due to velocity and the static lift due to the buoyancy force depending on the Froude number. In figure 7, the ratio $C_L/C^*_{L\,inf}$ as a function of the Froude number predicted by the linear

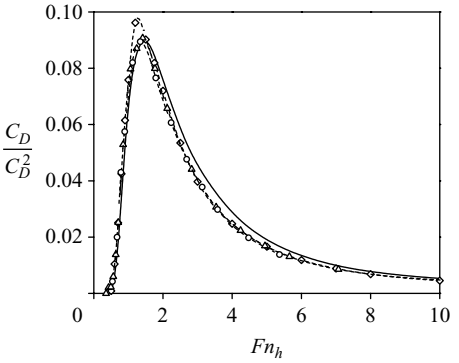

FIGURE 6. Ratio C_D/C_L^2 as a function of the submergence Froude number for the NACA 0012 hydrofoil at an angle of attack of 3° for various depths of submergence. Dashed lines: ⋄, $h/c = 1$; △, $h/c = 2$; ○, $h/c = 5$; solid line, dependence (3.3).

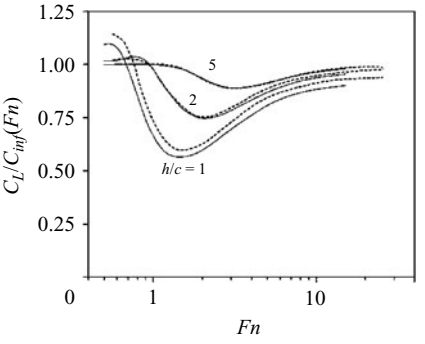

FIGURE 7. Comparison between the lift coefficient of the NACA 0012 hydrofoil obtained by the present nonlinear approach (solid lines) and the lift coefficient of a flat plate predicted by Hough & Moran's linear solution (dash lines) for various depths of submergence.

theory is compared with the ratio $C_L/C_{L\,inf}(Fn)$ obtained from the present nonlinear solution. Agreement is good for depths of submergence h/c of 2 and 5 while for depth $h/c = 1$, the nonlinear effects and the foil thickness lead to a somewhat greater reduction in the lift coefficient.

Figure 8 shows wave profiles past the NACA 0012 for various Froude numbers. As illustrated, the waves are sinusoidal in form, excluding some region near the foil. The relationship between the wave amplitude and the drag coefficient obtained from the solution agrees with that proposed by Salvesen (1969), $H/2 = Fn\sqrt{2C_D}$ (here, H is the wave height), so well that the discrepancy is less that 1%.

The results presented above show a good agreement between the linear and nonlinear theories concerning the force coefficients, the wavelength and amplitude in a wide range of Froude numbers.

4. Results for cavity flows

Cavitation may occur on a hydrofoil if the local pressure becomes lower than the vapour pressure of the liquid. Another case is ventilated cavitation, which is caused by gas injection into the low-pressure region on the foil. In both cases, the vapour/air bubble remains attached to the hydrofoil, which changes the flow geometry and

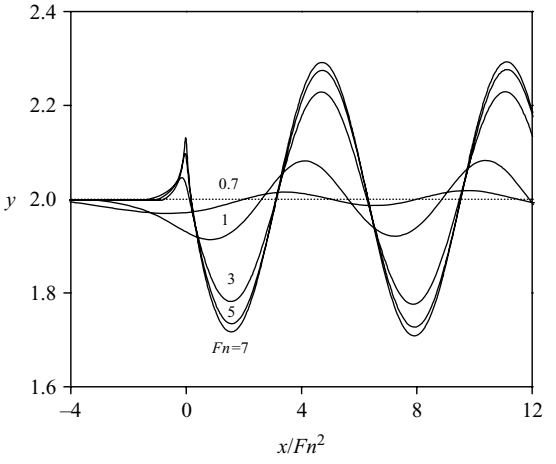

FIGURE 8. Froude-number effect on the wave profile past the NACA 0012 at incidence $\alpha = 3^\circ$ and depth of submergence $h/c = 2$.

leads to the loss of the leading-edge suction or forms drag, thus precluding the use of conventional hydrofoils similar to subsonic airfoils. Following Tulin & Burkart (1955), supercavitating hydrofoils are usually designed to have a sharp leading edge and a shaped wetted side providing a pressure peak near the trailing edge. The calculations presented below have been carried out for a cavitating flat plate as a simple case to study the effects of submergence, gravity, and cavitation development. The shape of a hydrofoil may be easily accounted for by including the integro-differential equation (2.14) into the calculation process.

Figure 9 indicates how the cavity streamlines and the free surface change as the hydrofoil approaches the free surface. As the depth of submergence decreases, the cavity becomes shorter and the free-surface elevation becomes greater. Such behaviour of the free surface increases the local angle of attack, say, at a one-chord distance upstream. Although the maximum elevation of the free surface decreases with depth, it starts to grow at a larger distance upstream. As the depth decreases, the jet formed by the free surface and the upper cavity contour becomes thinner and the pressure difference between the jet sides leads to a higher acceleration of the fluid directed inside the cavity. This increases the jet curvature and reduces the cavity length.

The cavity contours and the free surfaces for various Froude numbers at depth of submergence $h/c = 1.0$ are shown in figure 10. The gravity mostly affects the upper cavity contour and the free surface, and it does so in such a way that the thickness of the jet remains about constant. Since the gravity force acts in the same direction as the pressure difference between the jet sides, the cavity becomes shorter for a larger gravity or a smaller Froude number.

The cavitation number dependences of the cavity length for various Froude numbers are shown in figure 11. It is clearly seen that for Froude numbers $Fn < \infty$ the cavity length takes a finite value for zero cavitation number. In this case, the liquid jet is in a free fall in the gravitational field. As may be seen in figure 11, the greater the gravity (the smaller the Froude number), the shorter the cavity.

The Froude number dependences of the cavity length at zero cavitation number are shown in figure 12. It is the largest possible steady cavity in a fluid under gravity. If the pressure in the cavity is larger than the pressure at infinity at the same depth of submergence, then the pressure gradient accelerates the fluid at the cavity end

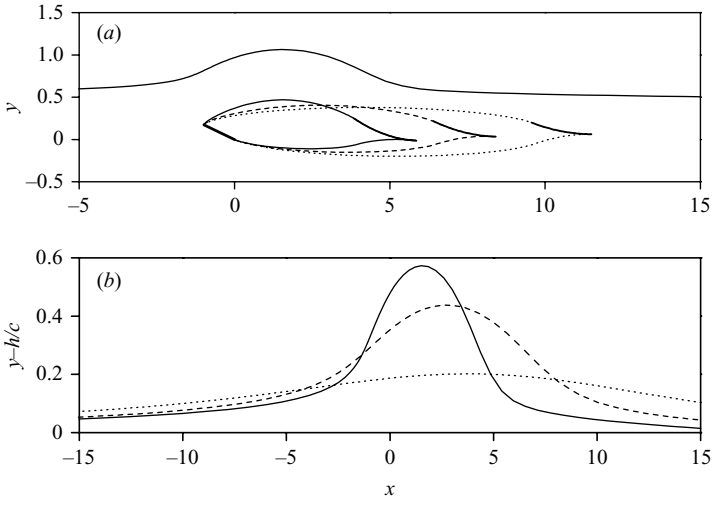

FIGURE 9. Effect of the depth of submergence on (*a*) the cavity contours and (*b*) free-surface elevation for a flat plate at incidence $\alpha = 10°$, Froude number $Fn = \infty$, and cavitation number $\sigma = 0.1$. Solid lines, $h/c = 0.5$; dashed lines, $h/c = 2$; dotted lines, $h/c = 10$. The free surface for $h/c = 0.5$ in (*a*) and (*b*) is the same free surface.

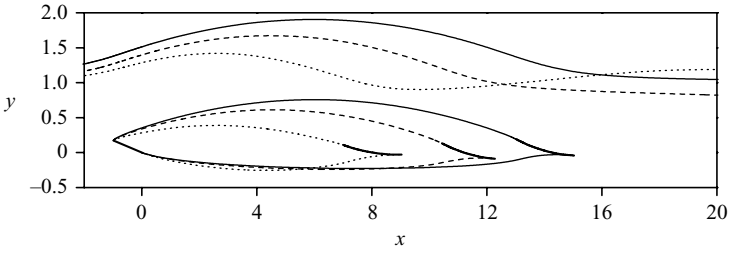

FIGURE 10. Effect of the Froude number on the cavity contours and the free surface for a flat plate at incidence $\alpha = 10°$, depth of submergence $h/c = 1.0$, and cavitation number $\sigma = 0.05$. Solid lines, $Fn = \infty$; dashed lines, $Fn = 5$; dotted lines, $Fn = 2$.

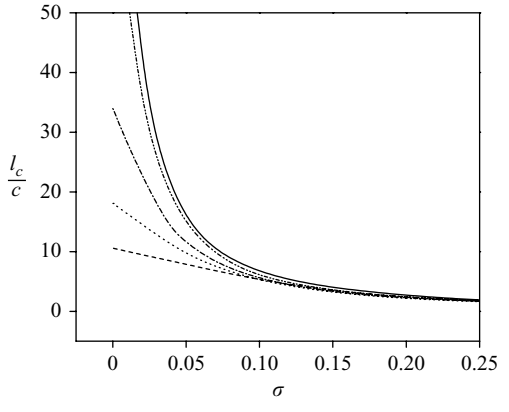

FIGURE 11. Effect of the Froude number on the cavitation-number dependence of the cavity length at depth of submergence $h/c = 1$. Solid line, $Fn = \infty$; dot dot dashed line, $Fn = 10$; dot dashed line, $Fn = 5$; dotted line, $Fn = 3$; dashed line, $Fn = 2$.

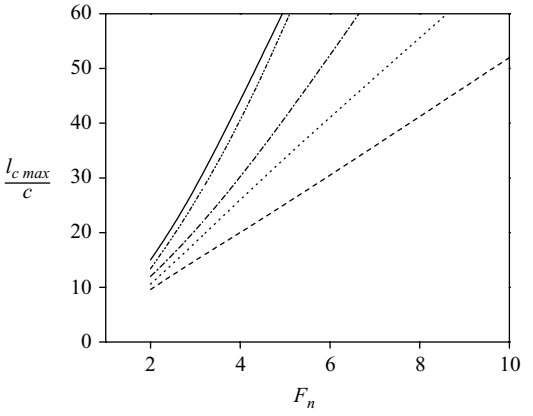

FIGURE 12. Cavity length at zero cavitation number versus Froude number for various depths of submergence. Solid line, $h/c = 10$; dot dot dashed line, $h/c = 5$; dot dashed line, $h/c = 2$; dotted line, $h/c = 1$; dashed line, $h/c = 0.5$.

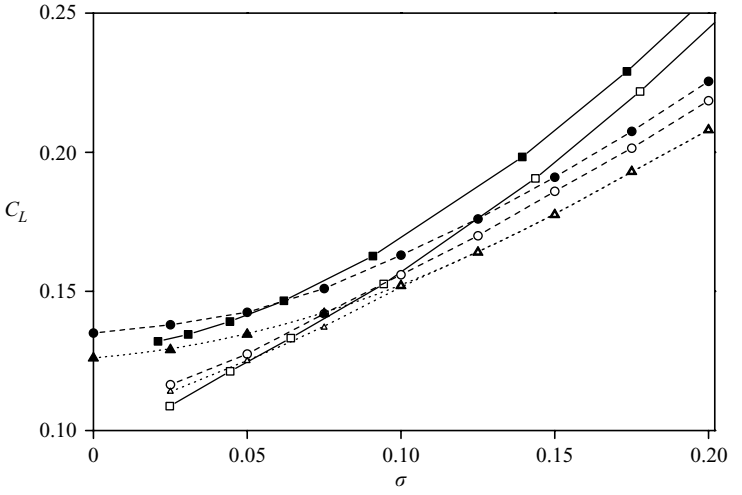

FIGURE 13. Lift coefficient predicted by the present theory (solid lines), Parkin's linear theory (dashed lines) and Larock & Street's nonlinear theory (dotted lines) for an unbounded flow region at incidence $\alpha = 5°$; solid symbols, $Fn = \infty$; open symbols, $Fn = 4$.

downstream and makes the cavity grow in size. As seen in figure 12, as the gravity tends to zero (the Froude number tends to infinity), the predicted maximum cavity length tends to infinity, which corresponds to the Kirchhoff flow in a weightless fluid. It should be noted that a finite cavity length in the presence of gravity at zero cavitation number was indicated by Tulin (1964).

Figure 13 shows the cavitation number dependences of the lift coefficient predicted by the present theory, Parkin's linear theory and Larock & Street's (1967*b*) nonlinear theory for an unbounded flow region and two values of the Froude number. The results of the present theory are calculated for the depth of submergence $h/c = 100$, at which free-surface effects are negligible. Note that for the case of a weightless fluid ($Fn = \infty$) there are some discrepancies between these theories, which become more pronounced for larger cavitation numbers. If for Parkin's fully linear theory this

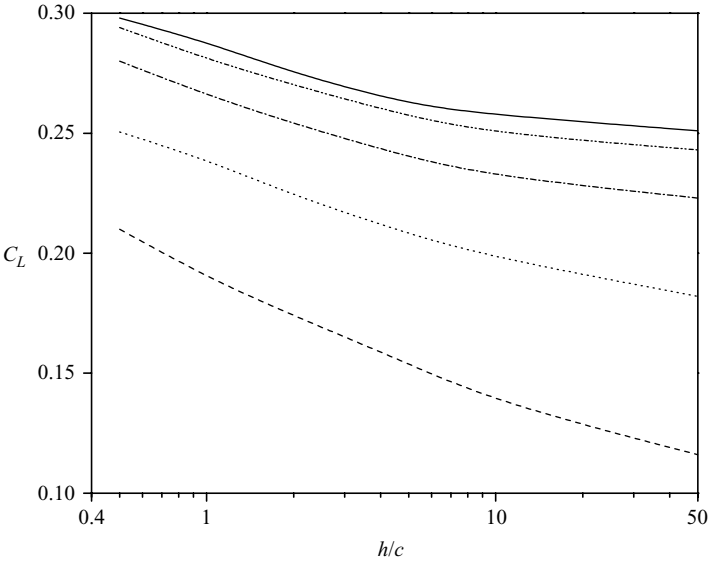

FIGURE 14. Effect of submergence on the lift coefficient at cavitation number $\sigma = 0.05$ and incidence $\alpha = 10^\circ$ for various Froude numbers; solid line, $Fn = \infty$; dot dot dashed line, $Fn = 10$; dot dashed line, $Fn = 5$; dotted line, $Fn = 3$; dashed line, $Fn = 2$.

discrepancy may be due to the linearization of the problem, then for the Larock & Street's nonlinear theory it may be due to numerical errors. We have also compared our results for the case of an infinite Froude number with the Wu (1962) results and found good agreement. As seen from figure 13, for the case of gravity with Froude number $Fn = 4$, all these theories agree for low cavitation numbers. For larger cavitation numbers, Parkin's linear theory and ours predict a similar lift reduction due to gravity, although the discrepancy in the lift coefficients increases. Larock & Street's results show lift reduction due to gravity only for small cavitation numbers $\sigma < 0.1$.

The effect of the free surface in the presence of gravity is shown in figure 14. As the foil approaches the free surface, the lift coefficient increases. This surface effect was studied using the linear theory by Johnson (1961) for a weightless fluid at zero cavitation number. He found the lift to increase from $0.5\pi\alpha$ to $\pi\alpha$ as the foil approaches the free surface. It is opposite to what occurs in the u cavitation-free regime, where the lift coefficient decreases from $2\pi\alpha$ to the same value $\pi\alpha$ (Bernicker 1966). Figure 9b shows the cause of the lift increase. The hydrofoil affects the free surface upstream and forms a liquid hill over the foil, which increases the local angle of attack.

An important feature is the negative slope of the dependence $C_L(h)$, which increases the probability of destabilization for a supercavitating hydrofoil craft. As seen from figure 14, gravity decreases the lift coefficient, but the slope of the dependence $C_L(h)$ remains almost the same as for the gravity-free case. This means that a hydrofoil craft with a submerged supercavitating foil system requires automatic control to keep the design depth of submergence. A similar type of instability requiring automatic control may occur for a hydrofoil craft with a subcavitating foil system operating in a waving seaway (Faltinsen 2005).

The Froude-number dependences of the lift coefficient are shown in figure 15 for various depths of submergence at incidence $\alpha = 10^\circ$ and cavitation number $\sigma = 0.05$.

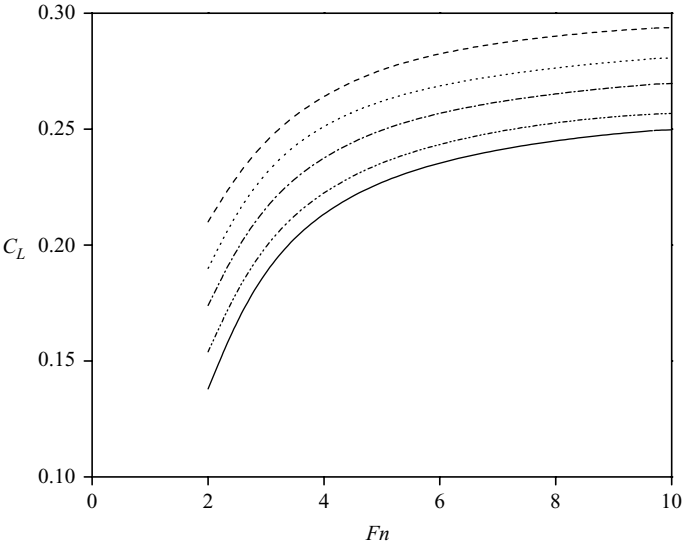

FIGURE 15. Effect of the Froude number on the lift coefficient at cavitation number $\sigma = 0.05$ for various depths of submergence. Solid line, $h/c = 10.0$; dot dot dashed line, $h/c = 5.0$; dot dashed line, $h/c = 2.0$; dotted line, $h/c = 1.0$; dashed line, $h/c = 0.5$.

This figure shows both the Froude number and submergence effects on the lift coefficient of a flat plate. Throughout the range of Froude numbers presented in figure 15, the lift decreases monotonically with decreasing Froude number. However, for very small Froude numbers, the lift should increase in just the same way as for cavity-free flows. Indeed, for small Froude numbers, the cavity length tends to zero for any cavitation number. This can be seen from figure 12 if we extrapolate the dependence of the maximum cavity length to $Fn < 2$. This means that the lift coefficient should be consistent with the results for the cavity-free flow presented in figure 7. The lift increase for small Froude numbers occurs because of the dominant effect of gravity on the free surface, which becomes flat and can be considered as a symmetry line of the flow. The velocity induced by the image foil leads to a larger angle of attack thus increasing the lift, and its influence increases for lower depths of submergence (Faltinsen 2005).

One of the earlier experimental investigations of cavitating hydrofoils near the free surface was by Dawson (1959). The experiments were carried out for a wedge shaped hydrofoil inside a free-surface water tunnel at an inflow velocity corresponding to Froude numbers in the range $F = 3.0 - 4.5$. To obtain a supercavitating flow for such a low inflow velocity, air was forced into the wake of the hydrofoil to form a constant pressure cavity. In figure 16, Dawson's experimental results are compared with the present theory and Wu's theory for a weightless infinite fluid. The presented results correspond to depth of submergence $h/c = 0.9$ and Froude number $Fn = 4$. We first note a good agreement between the present and Wu's theories, which looks surprising in the context of the results shown in figures 14 and 15. However, this agreement is just a happy occurrence due to a particular combination of the depth of submergence and the Froude number.

From figures 14 or 15 we can find that the lift coefficient for Froude number $Fn = 4$ and depth of submergence $h/c = 1$ is almost the same as for $Fn = \infty$ and $h/c = 50$. The experimental normal force coefficients for lower cavitation numbers agree very

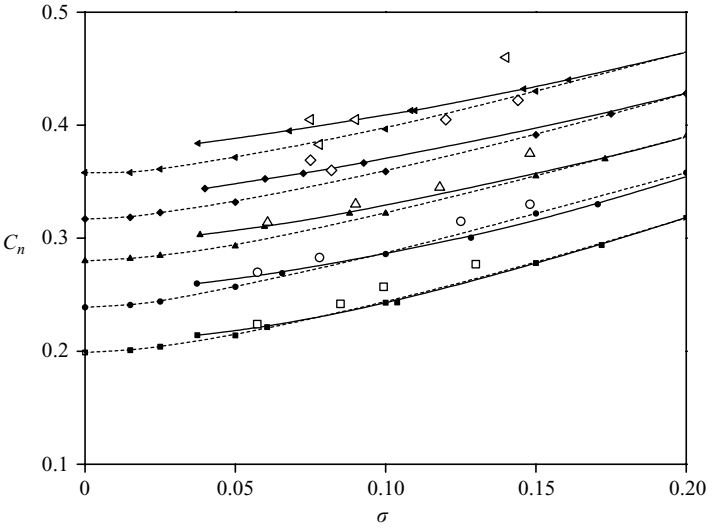

FIGURE 16. Cavitation-number dependences of the normal force coefficient for depth of submergence $h/c = 0.9$ and Froude number $Fn = 4$; the solid lines marked with the solid symbols correspond to the present calculations for angles of attack of 8°, 10°, 12°, 14° and 16° increasing from bottom to top; the same open symbols correspond to Dawson's experimental data; the dashed lines correspond to Wu's nonlinear theory for an unbounded flow region of a weightless fluid.

well with the present theory in a wide range of angles of attack. The larger the angle of attack, the more noticeable the discrepancy between Wu and the present theories, which is testimony to the influence of the free surface. However, agreement between the experimental data and the present theory remains good for all angles of attack.

Finally, we note that Froude numbers less than 10 and low cavitation numbers, say, $\sigma < 0.1$, can be realized in practice only for ventilated cavitation. From the definition of the cavitation and Froude numbers it follows that

$$Fn^2 = \frac{2}{\sigma}\left(\frac{(p_a - p_c)}{\rho g c} + \frac{h}{c}\right).$$

For example, if $h = c = 1\,\mathrm{m}$ and the pressure in the cavity is equal to the vapour pressure, $p_c = p_v \approx 0$, then $Fn = \sqrt{22/\sigma} = 10\sqrt{2.2}$ for $\sigma = 0.1$. On the other hand, if the pressure in the cavity is equal to, say, the atmospheric pressure, $p_c = p_a$, then $Fn = \sqrt{2/\sigma} \approx 4.5$ for the same value of the cavitation number.

5. Conclusions

An analytical solution of the cavitating flow past a hydrofoil beneath the free surface of a weighted fluid has been presented. The method employed leads to the derivation of an analytical expression for the complex flow potential defined in the first quadrant of the parameter plane. The solution provides a general nonlinear formulation for several problems considered in the literature separately, namely, for cavity and cavity-free flows past a hydrofoil beneath a free surface with and without gravity.

The proposed cavity closure model is a more adequate renewal of Wu's idea to simulate the actual flow at the cavity end within the framework of the ideal fluid

theory. Although this is not a major focus of our study, the proposed cavity closure model includes such important features as zero pressure gradient across the wake and the cavity closing at some distance downstream from the cavity end. The latter is an important feature for modelling cavity flows near the free surface. Besides, both partial cavitation and supercavitation are covered by the presented formulation.

The presented numerical results show how the cavity and free-surface shapes change as the hydrofoil approaches the free surface or/and the gravity increases in a wide range of depths of submergence and Froude numbers. Both the free surface and gravity result in shortening the cavity length. At the same time, they affect the lift coefficient in opposition to each other, which may diminish its change. The results obtained for the lift coefficient are in good agreement with experimental data.

As compared with a weightless fluid, gravity changes the flow pattern at zero cavitation number and provides a finite cavity length. This maximum possible length has been obtained for various Froude numbers and depths of submergence. As the gravity tends to zero, the maximum cavity length smoothly tends to infinity, which agrees with the gravity-free theory of ideal fluid.

The theoretical formulation of the present study includes the cavitation-free flow regime as the specific case where the cavity length is set to be zero. The results are reported in a wide range of Froude numbers in terms of the free-surface elevation, the wave profile, and the drag and lift coefficients. The obtained values of the combination C_D/C_L^2 are very close to the dependence $C_D/C_L^2 = 0.5/Fn\ \exp[-2/Fn_h]$ obtained by Kochin for a single vortex beneath the free surface using linearized boundary conditions on the free surface. Besides, the predicted wavelength downstream of the foil agrees with the length predicted by the linear theory. Thus, we may conclude that the nonlinear effects on the free surface affect the lift and drag coefficients only slightly, at least for the regimes in which the wave steepness is less than 0.1.

REFERENCES

Acosta, A. J. 1973 Hydrofoils and hydrofoil craft. *Annu. Rev. Fluid Mech.* **5**, 161–184.

Arakeri, V. 1975 Viscous effects on the position of cavitation separation from smooth bodies. *J. Fluid Mech.* **68**, 779–799.

Bernicker, R. P. 1966 A linearized two-dimensional theory for high-speed hydrofoils near the free surface. *J. Ship Res.* **10**, 25–48.

Chapman, S. J. & Vanden-Broeck, J.-M. 2006 Exponential asymptotics and gravity waves. *J. Fluid Mech.* **567**, 299–326.

Dagan, G. 1971 Free-surface gravity flow past a submerged cylinder. *J. Fluid Mech.* **49**, 179–192.

Dawson, T. E. 1959 An experimental investigation of a fully cavitating two-dimensional flat plate hydrofoil near a free surface. PhD thesis, California Institute of Technology, Pasadena.

Dias, F. & Vanden-Broeck, J.-M. 2003 On the internal fronts. *J. Fluid Mech.* **479**, 145–154.

Dias, F. & Vanden-Broeck, J.-M. 2004 Trapped waves between submerged obstacles. *J. Fluid Mech.* **509**, 93–102.

Duncan, J. 1983 The breaking and non-breaking wave resistance of a two-dimensional hydrofoil. *J. Fluid Mech.* **126**, 507–520.

Faltinsen, O. M. 2005 *Hydrodynamics of High-Speed Marine Vehicles*. Cambridge University Press.

Furuya, O. 1975 Nonlinear calculation of arbitrary shaped supercavitating hydrofoils near a free surface. *J. Fluid Mech.* **68**, 21–40.

Giesing, J. P. & Smith, A. M. O. 1967 Potential flow about two-dimensional hydrofoils. *J. Fluid Mech.* **28**, 113–129.

Gurevich, M. I. 1965 *Theory of Jets in Ideal Fluids*. Academic.

Havelock, T. H. 1926 The method of images in some problems of surface waves. *Proc. R. Soc. Lond.* A **115**, 268–280.

Helmholtz, H. 1868 Ueber discontinuirliche Flussigkeitsbewegungen. *Monasber. Berlin Akad.* pp. 215–228.

Hough, G. R. & Moran, J. P. 1969 Froude number effects on two-dimensional hydrofoils. *J. Ship Res.* **13**, 53–60.

Johnson, V. E., Jr, 1961 Theoretical and experimental investigation of supercavitating hydrofoils operating near the free water surface. *NASA TRR-93.*

Keldysh, M. V. & Lavrentiev, M. A. 1935 On the motion of a wing under the surface of a heavy fluid. *TsAGI, Moscow; translation in Science Translation Service, STS-75, Cambridge, MA, 1949.*

King, A. C. & Bloor, M. I. G. 1989 A semi-inverse method for free-surface flow over a submerged body. *J. Mech. Appl. Maths.* **42**, 183–202.

Kirchoff, G. 1869 Zur Theorie freier Flussigkeitsstrahlen. *J. reine u. angew. Math.* **70**, 289–298.

Kochin, N. E. 1937 On the wave resistance and lift of bodies submerged in a fluid. *TsAGI, Moscow; translation in SNAME Technical and Research Bulletin, 1951, pp. 1–8.*

Landrini, M., Lugni, C. & Bertram, V. 1999 Numerical simulation of the unsteady flow past a hydrofoil. *Ship Technol. Res.* **46**, 14.

Larock, B. E. & Street, R. L. 1967*a* A nonlinear solution for a fully cavitating hydrofoil beneath a free surface. *J. Ship Res.* **11**, 131–139.

Larock, B. E. & Street, R. L. 1967*b* A non-linear theory for a full cavitating hydrofoil in a transverse gravity field. *J. Fluid Mech.* **29**, 317–336.

Parkin, B. R. 1957 A note on the cavity flow past a hydrofoil in a liquid with gravity. *Engineering Division, California Institute of Technology, Pasadena, Rep.* 47-9.

Salvesen, N. 1969 On higher-order wave theory for submerged two-dimensional bodies. *J. Fluid Mech.* **38**, 415–432.

Schwartz, L. W. 1974 Computer extension and analytic continuation of Stokes' expansion for gravity waves. *J. Fluid Mech.* **62**, 553–578.

Semenov, Yu. A. & Cummings, L. J. 2006 Free boundary Darcy flows with surface tension: analytical and numerical study. *Euro. J. Appl. Math.* **17**, 607–631.

Semenov, Yu. A. & Iafrati, A. 2006 On the nonlinear water entry problem of asymmetric wedges. *J. Fluid Mech.* **547**, 231–256.

Smith, F. T. 1986 Steady and unsteady boundary-layer separation. *Annu. Rev. Fluid Mech.* **18**, 197–220.

Tuck, E. O. 1965 The effect of non-linearity at the free surface on the flow past a submerged cylinder. *J. Fluid Mech.* **22**, 401–414.

Tulin, M. P. 1964 The shape of cavities in supercavitating flows. *XI IUTAM Congress Paper, Munich, Germany.*

Tulin, M. P. & Burkart, M. P. 1955 Linearized theory for flows about lifting foils at zero cavitation number. *David W. Taylor Model Basin, Navy Dept. Rep. C-638.*

Vanden-Broeck, J.-M. 2004 Nonlinear capillary free-surface flows. *J. Engng. Maths.* **50**, 415–426.

Wilmot, P. 1987 On the motion of a small two-dimensional body submerged beneath surface waves. *J. Fluid Mech.* **176**, 465–481.

Wu, T. Y. 1962 A wake model for free-streamline flow theory. *J. Fluid Mech.* **13**, 161–181.

Zhukovskii, N. E. 1890 Modification of Kirchoff's method for determination of a fluid motion in two directions at a fixed velocity given on the unknown streamline. *Math. Coll.* **15**, 121–278.